

Key Points:

- Analog earthquake cycle experiments provide observations to evaluate the surface strain signals from the shallow megathrust
- The extensional segment of the forearc overlays the seismogenic zone at depth
- The strain state may remain quasi-stable over a few seismic cycles in the coastal zone

Supporting Information:

Supporting Information may be found in the online version of this article.

Correspondence to:

E. Kosari,
ehsan.kosari@gfz-potsdam.de

Citation:

Kosari, E., Rosenau, M., & Oncken, O. (2022). Strain signals governed by frictional-elastoplastic interaction of the upper plate and shallow subduction megathrust interface over seismic cycles. *Tectonics*, 41, e2021TC007099. <https://doi.org/10.1029/2021TC007099>

Received 3 OCT 2021

Accepted 15 APR 2022

© Wiley Periodicals LLC. The Authors. This is an open access article under the terms of the [Creative Commons Attribution License](#), which permits use, distribution and reproduction in any medium, provided the original work is properly cited.

Strain Signals Governed by Frictional-Elastoplastic Interaction of the Upper Plate and Shallow Subduction Megathrust Interface Over Seismic Cycles

Ehsan Kosari^{1,2} , Matthias Rosenau¹ , and Onno Oncken^{1,2} 

¹Helmholtz Centre Potsdam, GFZ German Research Centre for Geosciences, Potsdam, Germany, ²Department of Earth Sciences, Freie Universität Berlin, Berlin, Germany

Abstract The behavior of the shallow portion of the subduction zone, which generates the largest earthquakes and devastating tsunamis, is still insufficiently constrained. Monitoring only a fraction of a single megathrust earthquake cycle and the offshore location of the source of these earthquakes are the foremost reasons for the insufficient understanding. The frictional-elastoplastic interaction between the megathrust interface and its overlying wedge causes variable surface strain signals such that the wedge strain patterns may reveal the mechanical state of the interface. To contribute to this understanding, we employ Seismotectonic Scale Modeling and simplify elastoplastic megathrust subduction to generate hundreds of analog seismic cycles at a laboratory scale and monitor the surface strain signals over the model's forearc across high to low temporal resolutions. We establish two compressional and critical wedge configurations to explore the mechanical and kinematic interaction between the shallow wedge and the interface. Our results demonstrate that this interaction can partition the wedge into different segments such that the anelastic extensional segment overlays the seismogenic zone at depth. Moreover, the different segments of the wedge may switch their state from compression/extension to extension/compression domains. We highlight that a more segmented upper plate represents megathrust subduction that generates more characteristic and periodic events. Additionally, the strain time series reveals that the strain state may remain quasi-stable over a few seismic cycles in the coastal zone and then switch to the opposite mode. These observations are crucial for evaluating earthquake-related morphotectonic markers and short-term interseismic time series of the coastal regions.

1. Introduction

Estimating the interseismic coupling is the foremost approach to evaluate the earthquake potential of subduction megathrusts (Chlieh et al., 2008; Métois et al., 2013; Moreno et al., 2010; Schmalzle et al., 2014; Wallace et al., 2012). While both updip and downdip limits of megathrust ruptures are typically located offshore and near the shore, respectively, centuries-long recurrence intervals of the subduction megathrust earthquakes and geodetically insufficiently instrumented seafloors prevent us from achieving sufficient details of the shallow part of the megathrust (Kosari et al., 2020; Williamson & Newman, 2018). For instance, a weakly coupled interface had been predicted in NE Japan based on the incomplete and weakly constrained interseismic geodetic measurements before the 2011 Tohoku-Oki megathrust event (Loveless & Meade, 2011). However, the slip models of the earthquake itself derived from rare offshore geodetic data suggested a coseismic trench-breaching rupture (Ozawa et al., 2011; Simons et al., 2011; Sun et al., 2017). Besides short-term (geodetic) elastic surface deformation information, it is considered worthwhile to explore long-term (geologic) permanent deformation signals for potential diagnostic patterns linked to megathrust behavior (Geersen et al., 2018; Jara-Muñoz et al., 2015; Madella & Ehlers, 2021; Malatesta et al., 2021; Melnick et al., 2018; Molina et al., 2021; Normand et al., 2019; Ott et al., 2019; Saillard et al., 2017). Hence, for the sake of completeness of seismotectonic insights, long-term geological information should be referred to.

Elastoplastic deformation is the dominant process in the shallow portion of the subduction zones (Wang & Hu, 2006), and the mechanical properties of the wedge and megathrust govern the strain pattern in the upper plate. The strain signals could be accumulated over a single or many seismic cycles and preserved as morphotectonic features (i.e., extensional, compressional, and shear markers; Baker et al., 2013; Delano et al., 2017; Loveless et al., 2009; Rosenau & Oncken, 2009), representing the mechanical state of the forearc (Cubas et al., 2013a, 2013b). In an earthquake cycle, the mechanical state might be highly variable in the upper plate

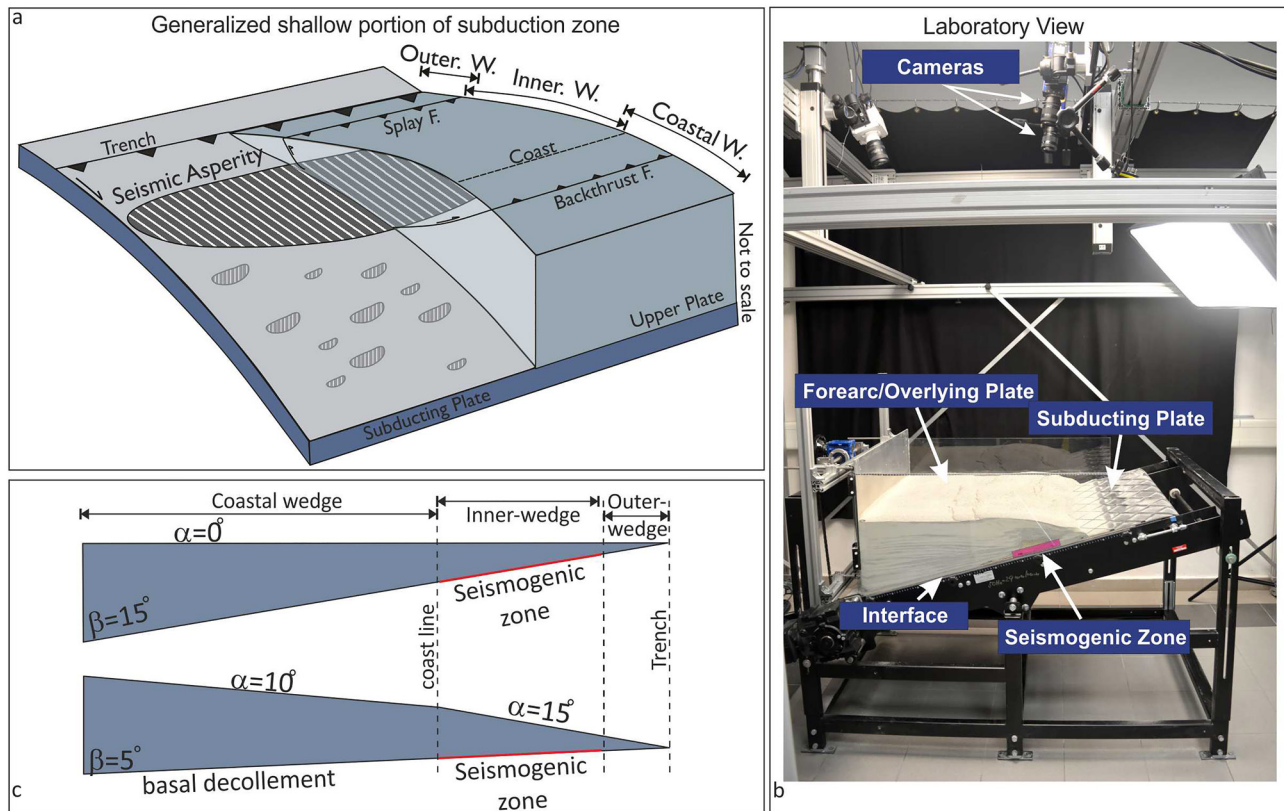


Figure 1. (a) Generalized shallow portion of the subduction zone. The structures in the upper plate and subducting plate are simplified. This schematic has been considered as a base for our analog seismotectonic model. (b) Laboratory view of our experiment. The main part of the analog model is labeled in the image. (c) 2-D view of the two evaluated configurations in this study. The projection of the downdip limit of the stick-slip material is defined as the coastal area. Alpha (α) and beta (β) represent the surface slope and basal decollement dip, respectively.

(Kopp, 2013; Melnick et al., 2009). In other words, the interaction between the rate-strengthening (creeping) and rate-weakening (seismogenic) portions of the megathrust and the overriding plate cause time and space variable strain fields and rates over the forearc during a seismic cycle. For instance, the coastal region can typically be under compression during the interseismic period and under extension during and immediately following the coseismic stage (e.g., Wang et al., 2019). Understanding how this leads to coastal topography and offshore bathymetry as a persistent marker over many seismic cycles is vital. Eventually, this may lead to incremental upper plate evolution toward its critical geometry and shape the forearc morphology (Cubas et al., 2013a, 2016; Wang & Hu, 2006).

We may not fully infer the seismic potential of the shallow (offshore) portion of the megathrust via only onshore observations. Furthermore, the potential temporal linkage between strain states (elastic and plastic) at the positions of the coast, inner-wedge, and outer-wedge is not resolved. Finally, could permanent surface deformation (i.e., plastic strain) be reliably used as a clue for inferring the zones with megathrust earthquake potential? In an attempt to answer these questions, we employ Seismotectonic Scale Modeling (Rosenau et al., 2009, 2017) to generate physically self-consistent analog megathrust earthquake ruptures and seismic cycles at the laboratory scale (Figure 1).

This method has been used to study the interplay between short-term elastic (seismic) and long-term permanent deformation (Rosenau & Oncken, 2009). For mimicking the megathrust seismic cycle and its associated surface deformation, we use a zone of velocity weakening (stick-slip) material and an elastoplastic wedge while the wedge is continuously compressed via a basal conveyor belt (Kosari et al., 2020; Rosenau et al., 2019). A stereoscopic image correlation technique has been used to monitor the surface deformation of the analog model (Adam et al., 2005). Generating hundreds of seismic cycles and monitoring the associated surface deformation allow us to unwrap the surface signals related to frictional properties at depth (velocity weakening versus velocity neutral).

2. Seismotectonic Scale Modeling and Monitoring Techniques

Seismotectonic Scale Modeling is a unique technique to forward model the tectonic evolution over seismic cycles (e.g., Rosenau et al., 2017, and references therein). The approach has been used to study the interplay between short-term elastic (seismic) and long-term permanent deformation (Rosenau & Oncken, 2009), earthquake recurrence behavior and predictability (Corbi et al., 2017, 2019, 2020; Rosenau et al., 2019), the linkage between offshore geodetic coverage and coseismic slip models (Kosari et al., 2020), and details of the seismic cycle (Caniven & Dominguez, 2021). Analog models are downscaled from nature for the dimensions of mass, length, and time to maintain geometric, kinematic, and dynamic similarity by applying a set of dimensionless numbers (King Hubbert, 1937; Rosenau et al., 2009, 2017). The models generate a sequence of tens to hundreds of analog megathrust earthquake cycles, allowing the analysis of the corresponding surface displacement from dynamic coseismic to quasi-static interseismic stages.

In the 3-D experimental setup introduced in Kosari et al. (2020), a subduction forearc model is set up in a glass-sided box (1,000 mm across strike, 800 mm along strike, and 300-mm deep) on top of an elastic basal rubber conveyor belt (the model slab), and a rigid backwall. A wedge made of an elastoplastic sand-rubber mixture (50 vol.% quartz sand G12: 50 vol.% EPDM-rubber) is sieved into the setup representing a 240 km long forearc segment from the trench to the volcanic arc position (Figure 1).

At the base of the wedge, zones of velocity weakening controlling stick-slip (“seismic” behavior) are realized by emplacing compartments of “sticky” rice (“seismogenic zone”), which generate quasi-periodic slip instabilities while sheared continuously (Figure 1), mimicking megathrust earthquakes of different size and frequency. Large stick-slip instabilities are assumed to represent almost complete stress drops and recur at low frequency (~ 0.2 Hz) at a prescribed constant convergence rate of 50 $\mu\text{m/s}$. This stick-slip behavior is intended to mimic rare great (M8–9) earthquakes (Kosari et al., 2020; Rosenau et al., 2019) with century-long recurrence intervals. The wedge itself and the conveyor belt respond elastically to these basal slip events, similar to crustal rebound during natural subduction megathrust earthquakes. Upper plate faults (in our case, an “inland” backthrust fault and “offshore” forethrust and backthrust faults) emerge self-consistently downdip and updip of the seismogenic zone due to time-dependent frictional variations across its limits which change polarity over seismic cycles, causing switches between local transient compression and extension as documented in earlier papers (Kosari et al., 2020; Rosenau & Oncken, 2009; Rosenau et al., 2010).

The Coulomb wedge theory considers the mechanics of a wedge that evolves into a critical geometry while the fault slips at constant shear stress and the wedge is in a critical state (Dahlen et al., 1984; Davis et al., 1983). This theory can also be applied to the seismic cycle cases in which the fault alternates between interseismic locking and coseismic slip to assess the temporal changes in the state of stress and deformation mechanism over seismic cycle (Wang & Hu, 2006). According to this theory (Dahlen et al., 1984), two different types of wedge configurations have been designed: a “compressional” configuration represents an interseismically compressional and coseismically stable wedge, and a “critical” configuration, which is interseismically stable (close to compressional criticality) and may reach extensional criticality coseismically depending on how large the dynamic friction drop is (Figure 2). In the compressional configuration, a flat-top ($\alpha = 0$) elastoplastic wedge overlies a single large rectangular in map view stick-slip patch (Width \times Length = 200 \times 800 mm) over a 15-degree dipping basal thrust. In the critical configuration, the surface angle of the elastoplastic wedge varies from the inner-wedge ($\alpha = 10$) to the outer-wedge ($\alpha = 15$) over a 5-degree dipping basal thrust. The stick-slip patch has the same dimension in both configurations, and so transient stresses associated with the time-dependent frictional variation across its limits are the same. The stick-slip zone in both configurations represents a system of a homogeneous seismogenic zone with a temperature-controlled depth range and no variation along strike generating M9 type megathrust events (Figure 1). The shallow wedge (Figure 2, w2) of the compressional configuration overlying the seismogenic zone is compressional in the interseismic stage when the basal friction in the seismogenic zone is relatively high, and stable during the coseismic stage when the basal friction in the seismogenic zone drops to low values. The coastal part of the wedge in the compressional configuration (w1) is compressional throughout the seismic cycle.

The critical configuration, in contrast, has a coastal wedge (w3) that is critical throughout the seismic cycle, whereas the shallow wedge (w4) overlying the seismogenic zone is stable interseismically but becomes critically extensional during the coseismic stage (Figure 2).

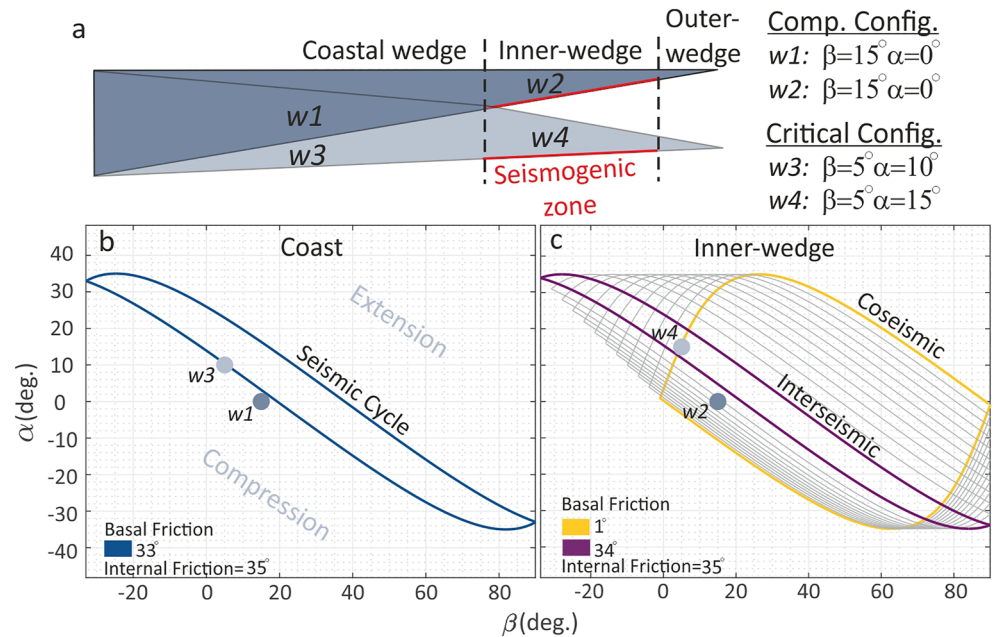


Figure 2. Mechanical states of a wedge introduced by the critical taper theory for interseismically compressional and critical experiments. (a) Location of the coastal wedge (w1 and w3) and inner-wedge (w2 and w4) on the schematics of the compressional and critical configurations. The surface slope and basal decollement dip for both experiments are marked as alpha (α) and beta (β). Lower panel shows the mechanical states of the coastal wedge (b) and the inner-wedge (c). The values from basal friction and internal friction are adopted from the ring-shear test (Figure S1 in Supporting Information S1). The areas within the envelopes characterize stable regimes. The areas above and below the envelopes indicate extensional and compressional regimes, respectively. The positions on the envelopes represent critically stable domains.

To capture horizontal micrometer-scale surface displacements associated with analog earthquakes and interseismic intervals at microsecond scale periods, a stereoscopic set of two CCD (charge-coupled device) cameras (LaVision Imager pro X 11MPx, 14 bit) images the wedge surface continuously at 4 Hz. To derive observational data similar to those from geodetic techniques, i.e., velocities (or incremental displacements) at locations on the model surface, we use digital image correlation (DIC; Adam et al., 2005) via the DAVIS 10 software (LaVision GmbH, Göttingen/DE) and derive the 3-D incremental surface displacements at high resolution (<0.1 mm; Figure 3).

3. Results and Interpretations

The observations are presented in succession from long-term to short-term. First, we show how the upper plate structures evolve in a sequence over hundreds of analog earthquake cycles. We evaluate the spatial correlation between upper plate strain (Text S1 in Supporting Information S1) and topography evolution regarding locking and slip at the interface. Afterward, we spatially and temporally zoom in on a subset of seismic cycles to explore how strain states vary in different segments of the upper plate across seismic cycles. Eventually, the strain cycles in different wedge segments (i.e., outer-wedge, inner-wedge, and coast) are compared to assess how similar they respond to the earthquake cycles in a homogeneous wedge with internal discontinuities (i.e., upper plate faults).

3.1. Model Evolution From Long to Short Time Scales

3.1.1. Wedge Anatomy: Final Geometry, Surface Strain Distribution, and Structures Formed

The cumulative plastic strain pattern maps illustrate the final (hundreds of analog earthquake cycle) strain distribution in the upper plate (Figure 4). In the compressional and the critical configurations, surface strain patterns represent three different segments: a compressional domain in the outer-wedge, an extensional domain in the inner-wedge, and a compressional domain in the coastal wedge. The outer-wedge compressional segment overlies the shallow creeping portion of the interface. Further rearward, the compression domain grades into

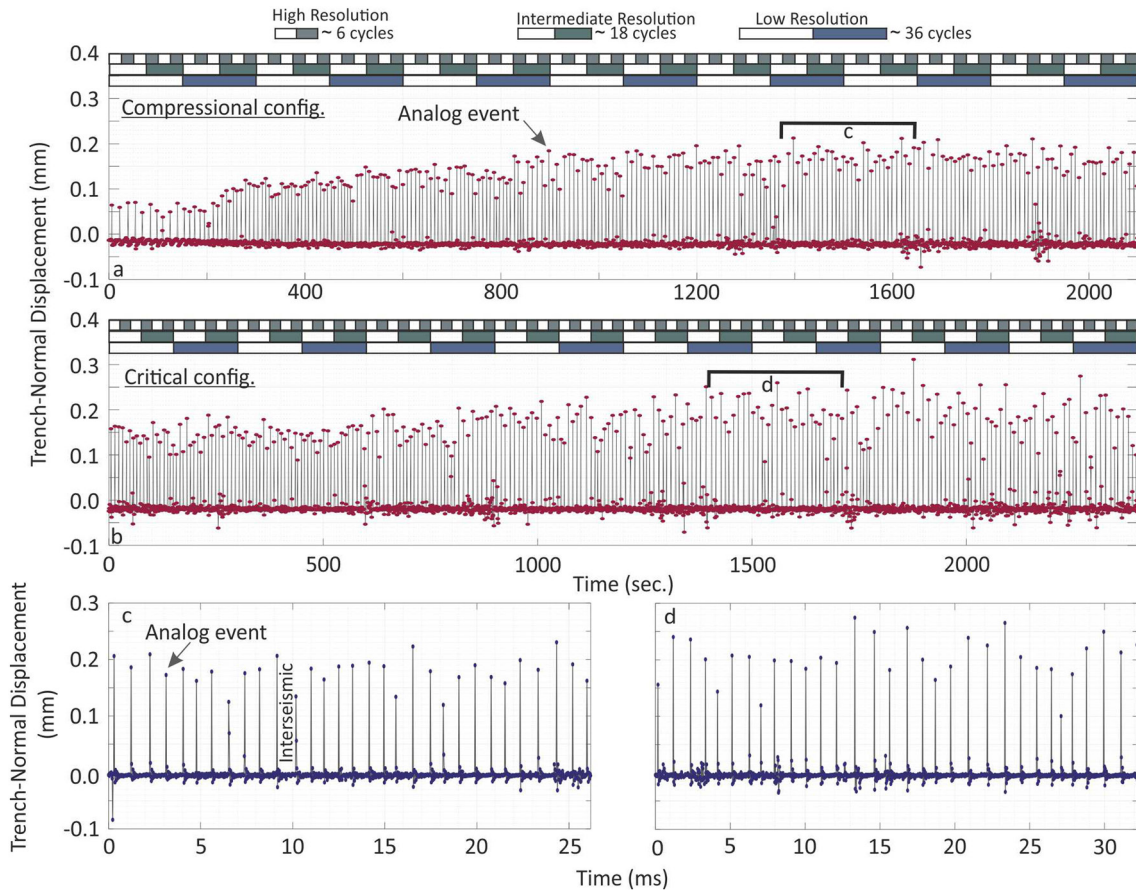


Figure 3. Analog earthquake catalog derived from surface displacement above the stick-slip zone on the model surface. The displacements larger than 0.05 mm represent an analog megathrust event ($M_w \geq 8$ at nature scale). Distance between two analog events represents the interseismic period in our experiments. (a and b) All the events that occurred over model evolution from compressional and critical configurations, respectively. Temporal processing windows for three different resolutions are differentiated by scale bars (see Figures 6 and 7 for more details). (c and d) A selected set of 30–32 analog megathrust events for evaluating surface displacement over the seismic cycles from both configurations.

an extensional domain in the inner-wedge overlying the velocity-weakening zone on the interface at depth. In our experiments, two main mechanisms could cause the plastic extensional strain in the inner-wedge: A minor anelastic component of the mainly elastic coseismic extension and the activity of splay fault-related folds. A compressional segment has also been observed in the coastal wedge, which may appear on the model's surface as a backthrust fault rooting in the frictional transition zone at the downdip limit of the velocity-weakening zone (Figures 4 and 5). The backthrust fault is not sharply visible in the total surface deformation map (Figure 4) due to the high strain gradient at the deformation front (i.e., trench zone and forethrust splay fault), but the fault can be followed in the deformation maps generated over dozens of analog earthquake cycles (Figure S2 in Supporting Information S1) and in the final surface topography (Figure 6a).

In both configurations, localization of deformation has segmented the upper plate into three main segments. The outer-wedge is underthrust and subsided. The inner-wedge, which is bounded by the updip splay fault and downdip backthrust fault, has accumulated the deformation during seismic cycles through internal deformation and vertical displacement due to the activity of the backthrust faults. Further rearward (landward), subsidence occurs in the footwall of the backthrust fault (Figure 4) the subsiding area in the coastal wedge is relatively wider in the compressional configuration (Figure 4c and Figure S2 in Supporting Information S1).

Both compressional and critical configurations demonstrate uplift and extension above the seismogenic zone embraced by shortening domains inland and near the trench. However, the compressional domain further rearward (coastal wedge) is smaller in the critical configuration. Close to the trench, conversely, the upper plate shortens and subsides. In the compressional configuration, the shortening in the transition zone from the shortening

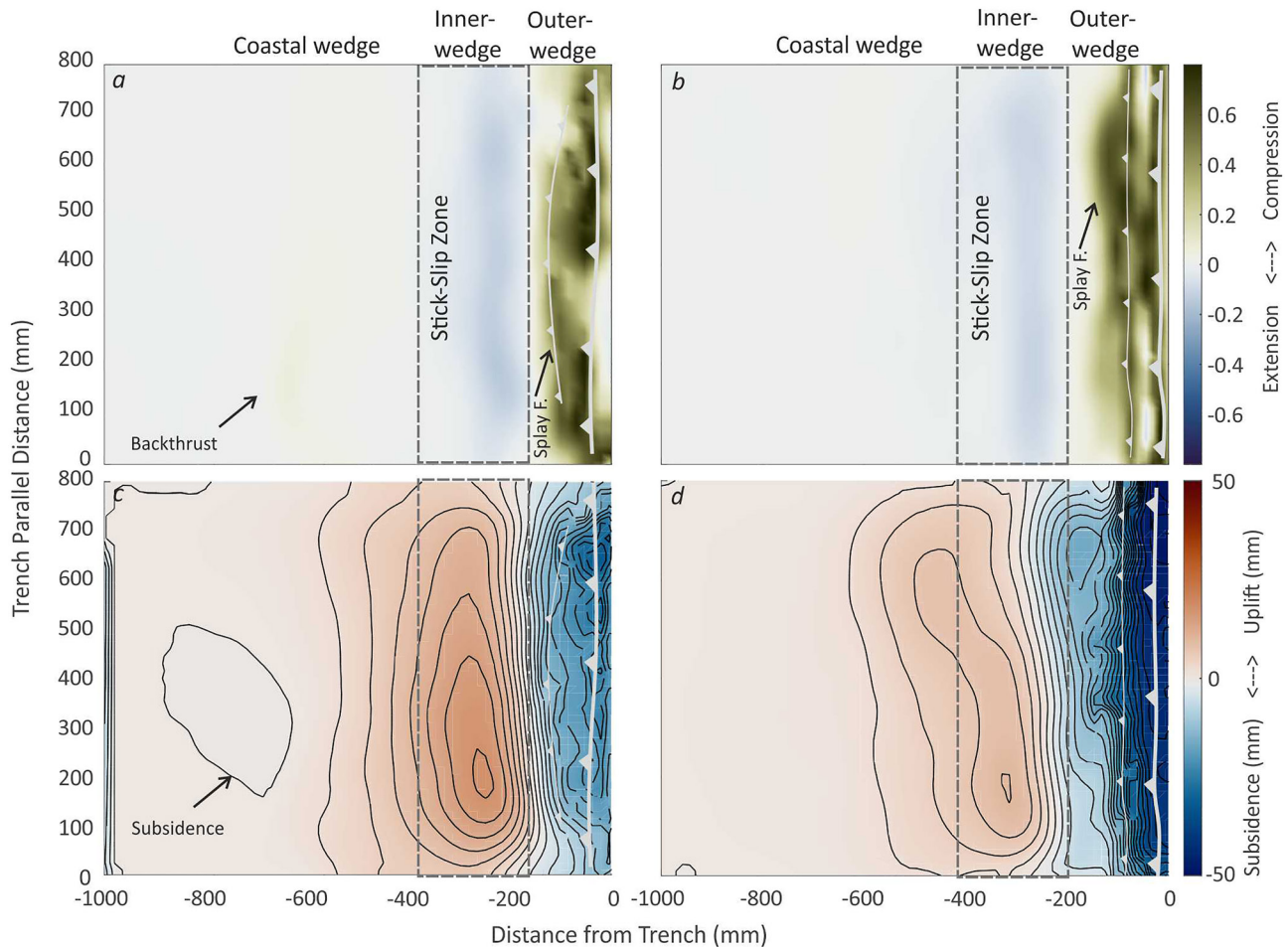


Figure 4. Total surface deformation maps (after hundreds of seismic cycles) from compressional (a and c) and critical (b and d) configurations. The approximate location of the stick-slip zone at depth is projected on the model surface as a dashed rectangle. (a and b) Surface strain maps from both configurations. Green and blue represent compression and extensional domains, respectively. The outer-wedge experiences (splay fault and trench domains) compression. Inner-wedge records permanent extension. The activity of the backthrust is dimly visible in the compressional configurations. The location of the fault can be sharply followed in Figure S2 in Supporting Information S1 and Figure 5. (c and d) Permanent vertical deformation in the absence of erosion in the system. The outer-wedge and inner-wedge represent permanent subsidence and uplift, respectively. The weak subsidence zone onshore may represent a forearc basin at the natural scale.

domain to the extension domain is accommodated by a pop-up structure forming a conjugated forethrust and backthrust couple (Figure 5). Although the pop-up structure remains temporarily active, it generates a local surficial extension domain between its boundary faults (Figure 5c). In the critical configuration, the forethrusts are the only structures accommodating forearc shortening. In the compressional configuration, the backthrust fault rooted at the downdip of the stick-slip zone is the main structure accommodating wedge shortening.

3.1.2. Upper Plate Faults Formation Over Model Evolution

During model evolution, the first structures appear in the vicinity of the deformation front (near the trench). In the compressional configuration, near the trench, a trenchward-dipping (backthrust) and a rearward-dipping (forethrust) thrust faults form shortly after each other. These two trench-parallel faults, which likely conjugate at depth, create a ridge-shaped structure (Figures 5a and 5c).

The structures are formed above the upper basal frictional transition. The stick-slip (seismogenic) zone represents high basal friction in a long-term (interseismic) interval relative to the uppermost portion of the interface, which creeps interseismically. This frictional contrast thus leads to a sharp slip rate variation and stress concentrations along the interface where the thrusts nucleate. Another active trenchward-dipping thrust fault (backthrust) forms further rearward in the wedge, representing the onshore segment of the forearc (coastal wedge). Again, the frictional contrast between the velocity-weakening portion of the interface (seismogenic zone) and the downdip limit

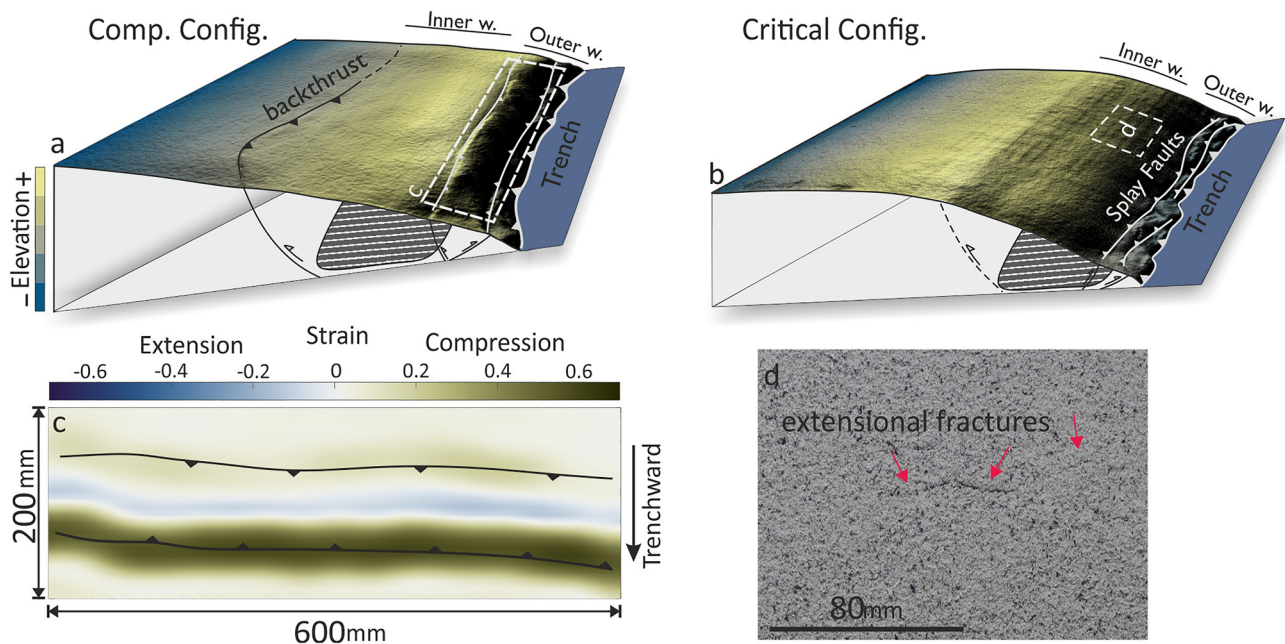


Figure 5. Final surface topography of compressional (a) and critical (b) configurations. The backthrust and the splay faults are rooted in the downdip and updip limits of the stick-slip zone. The splay faults separate the outer-wedge from the inner-wedge. The surface exposure of the backthrust is only visible in compressional configuration. The strain field generated by the activity of the splay faults is visualized in (c). The ridge-shape structure represents extensional strain. Examples of the surface coseismic extensional fracture are shown in panel (d).

of this portion controls the origin of the backthrust, thereby accommodating the difference in slip rate (Figures 5 and 6). The thrust system accommodates shortening, causing uplift and steepening of the wedge over the course of the experiment consistent with the predicted transiently compressional initial geometry.

In the critical configuration, a splay forethrust forms at the updip limit of the seismogenic zone (Figure 5). In contrast to the compressional wedge, a backthrust does not form at the downdip limit of the seismogenic zone consistent with its stable geometry according to Coulomb wedge theory. These faults show thrust mechanisms and form in the immediate updip and downdip parts of the seismogenic zone.

3.1.3. Long-Term Wedge Deformation: Long-Term Surface Displacement Signals Reflecting Forearc Evolution

To visualize the long-term behavior (i.e., integrating multiple seismic cycles) of the forearc wedge, the differential surface displacement (horizontal and vertical) covering 18, 9, and 3 megathrust analog earthquake cycles (Figures 6 and 7) are visualized. This illustrates how the wedge evolution is recorded by observational data with different temporal resolutions typical of geomorphological methods (e.g., terrace uplift).

In both configurations, the long-term vertical displacement can be temporally divided into two parts depending on whether the upper plate faults are active or inactive. In the case of an active splay fault, the horizontal trenchward displacement terminates at the location of the splay fault, and the zone of maximum uplift is in the hanging-wall of the splay fault (Figures 6 and 7). The splay fault activity decreases over time until it dies, and subsequently, the whole slip is consumed on the interface (i.e., megathrust). Namely, a nontrench-reaching megathrust earthquake system turns into a trench-reaching system over time (Figure S4 in Supporting Information S1). The evolution of the backthrust can also be tracked in all temporal resolutions of topography evolution derived from the compressional configuration (Figure 6). The zone of maximum topography correlates with the zone of the maximum extensional segment of the upper plate in both configurations. In the compressional configuration, this extensional zone becomes wider and more pronounced over time, while the width of the zone remains relatively constant over time in the critical configuration.

Further rearward to the coastal wedge, the strain evolves differently in the compressional and critical configurations: In the compressional configuration, the initially extensional strain is replaced by a compressional domain

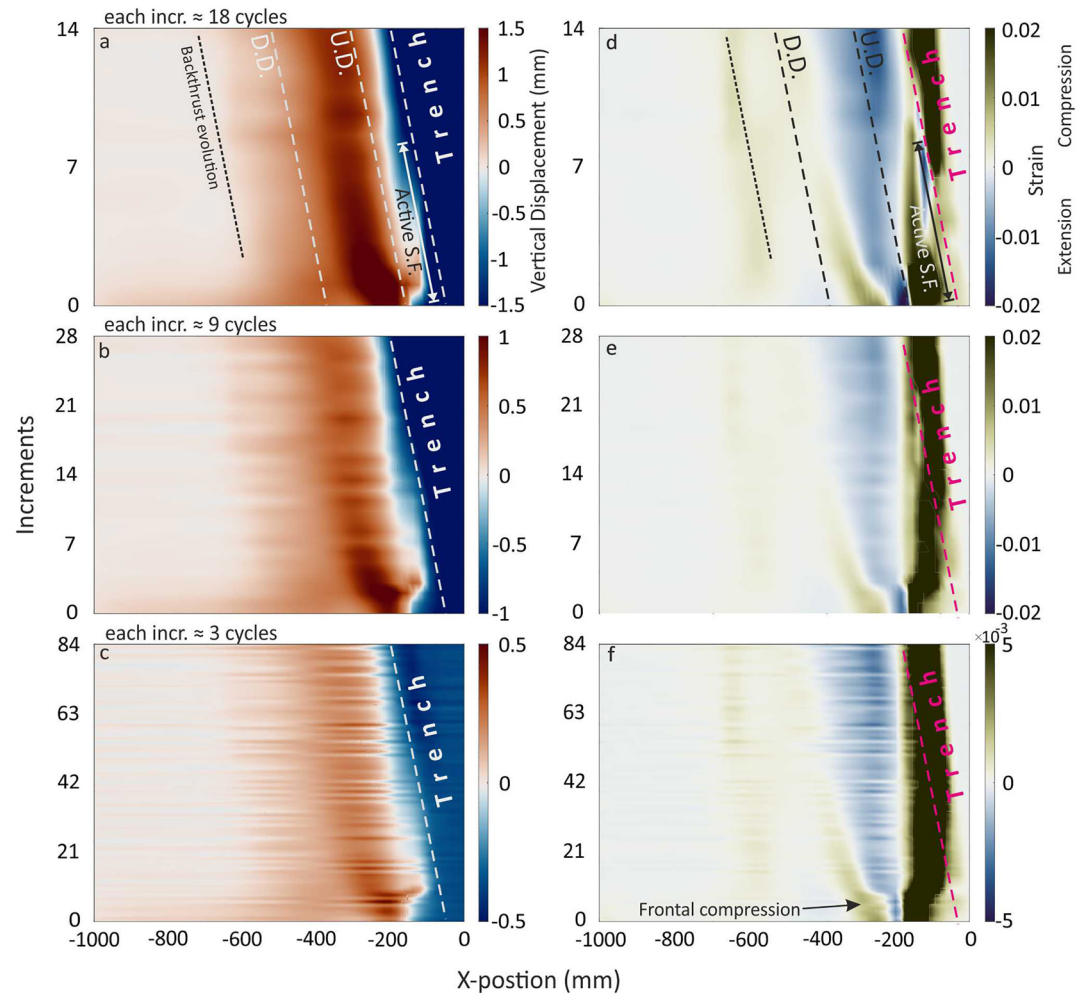


Figure 6. Incremental surface vertical displacement and strain over model evolution from the compressional configuration with different temporal resolutions (3, 9, and 18 analog earthquake cycles). Updip (UD) and downdip (DD) of the stick-slip zone at depth have been projected on the surface. (a)–(c) represents vertical uplift (warm color) and subsidence (cold color). The activity of the splay fault (SF) is evident while it is gradually deactivated and the whole slip is transferred on the megathrust. (d)–(f) represents surface strain maps with different temporal resolutions. Note that the transient uplift and strain pattern and large temporal deformation due to large analog earthquake are only visible in the observation with high temporal resolution (c and f).

over the entire inner-wedge. The maximum compressional strain appears in the coastal wedge where the backthrust is formed. The frontal compressional domain diminishes while the compressional wedge is evolving. This is in good agreement with the activity of the updip splay fault over its lifetime. The strain pattern over the inner-wedge illustrates that this wedge segment gradually evolves to a more compressional regime. In contrast, there is no significant frontal compressional domain in the critical configuration (Figure 7), and the inner-wedge is rather in an extensional state. Although the coastal wedge in the critical configuration similarly shows a compressional state, the backthrust fault does not appear in the wedge at the downdip limit of the stick-slip zone.

3.1.4. Short-Term Wedge Deformation: Strain Pattern Over Seismic Cycles

3.1.4.1. Extensional Features in the Shallow Segment of the Forearc

The extensional features have generally been observed as extensional fractures or/and crestal normal faults in the frontal wedge domain of the models (Figure 5 and Figure S3 in Supporting Information S1). The latter may form above the frictional transition zone at the updip limit of the velocity-weakening zone. The activity of the forethrust splay faults plays the main role in their formation being located in the crestal zone in the hanging-wall of the splay fault. This fracture zone reflects the splay fault's activity and, consequently, the updip limit (frictional transition)

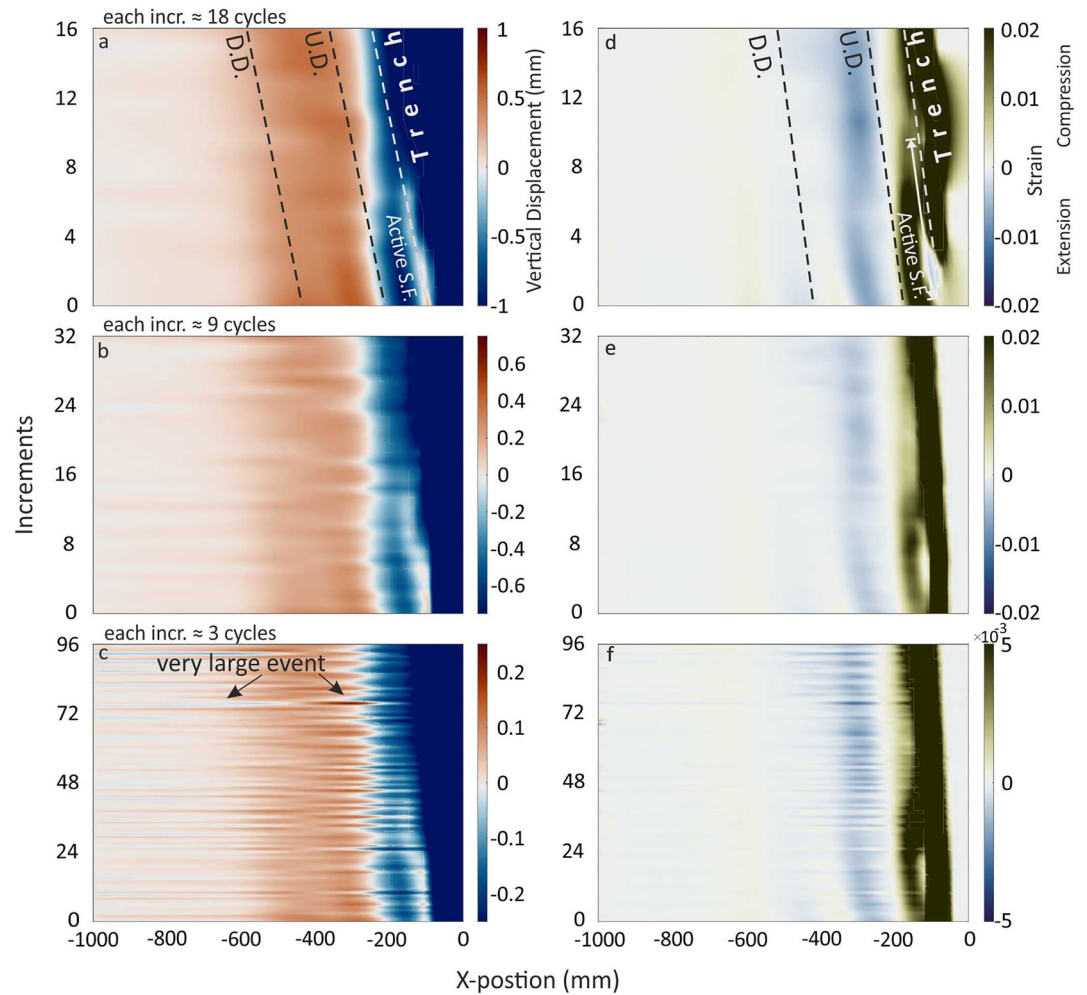


Figure 7. Incremental surface vertical displacement and strain over model evolution from the critical configuration with different temporal resolutions (3, 9, and 18 analog earthquake cycles). Updip (UD) and downdip (DD) of the stick-slip zone at depth have been projected on the surface. (a)–(c) represents vertical uplift (warm color) and subsidence (cold color). The activity of the splay fault (SF) is evident while it is gradually deactivated and the whole slip is transferred on the megathrust. (d)–(f) represents surface strain maps with different temporal resolutions. Note that the transient uplift and strain pattern and large temporal deformation due to large analog earthquakes are only visible in the observation with high temporal resolution (c and f).

of the velocity-weakening portion of the interface. The extensional features form and develop trench-parallel inelastically over the interseismic interval and are active in opposite modes during the coseismic and postseismic stages, i.e., coseismically extensional and postseismically compressional. The responsible mechanism of the extensional features is the activity of the splay forethrust forming fault-related folds (Figure S3 in Supporting Information S1).

Consequently, a local extensional regime forms at the hinge zone of the fault-related fold and may lead to the crestal normal faults (i.e., extrado). In the coseismic interval, a sudden slip on the splay fault and megathrust enhances these extensional fractures. The slip on the faults terminates at the frictional transitional border. Hence, a compressional strain regime appears in the forelimb of the fault-related fold.

The fractures appear in the inner-wedge segment of the model forearc where they overlay the velocity-weakening portion of the interface at depth. The extensional fractures in the inner-wedge above the seismogenic zone form coseismically, where the maximum extensional strain occurs in the forearc and is partially preserved as anelastic deformation in each earthquake cycle. In contrast, during the interseismic period, this segment of the forearc is mainly under compression.

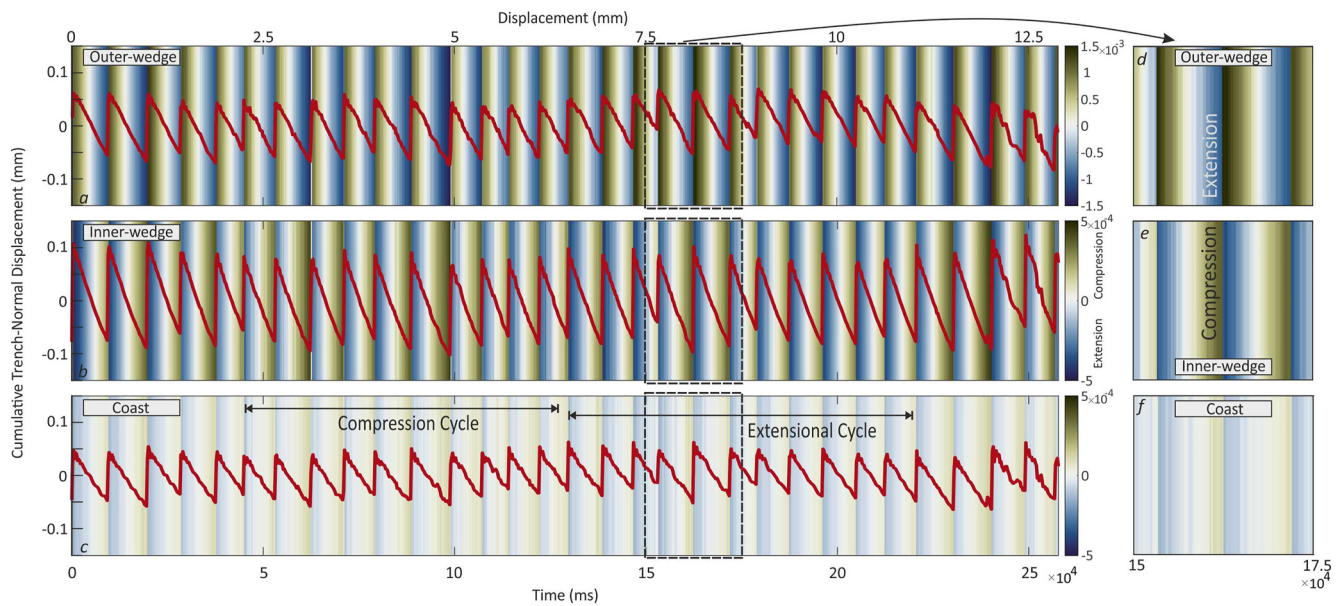


Figure 8. Compressional configuration; trench-normal displacement time series (red plot) is overlaid on the strain time series (background color map) over tens of analog earthquake cycles in different segments of the upper plate. The magnitude of the strain in the outer-wedge is one order larger than the inner-wedge and coast. Note that the outer-wedge and inner-wedge show opposite strain states over the earthquake cycle (compressional versus extensional). The compression and extensional supercycles in the coastal region are shown in the lower panel. Please see the text for the discussion.

3.1.4.2. Strain-State Cycle Over the Seismic Cycle

Here, we have visualized the average value of the strain over three different segments of the forearc to take a closer look at the strain evolution at the time scale of individual seismic cycles (Figures 8 and 9). In general, the strain rate reduces rearward from the trench toward the coast, consistent with the dominance of elastic loading at the seismic cycle time scale. The outer-wedge shows strains opposite to those of the coast and inner-wedge

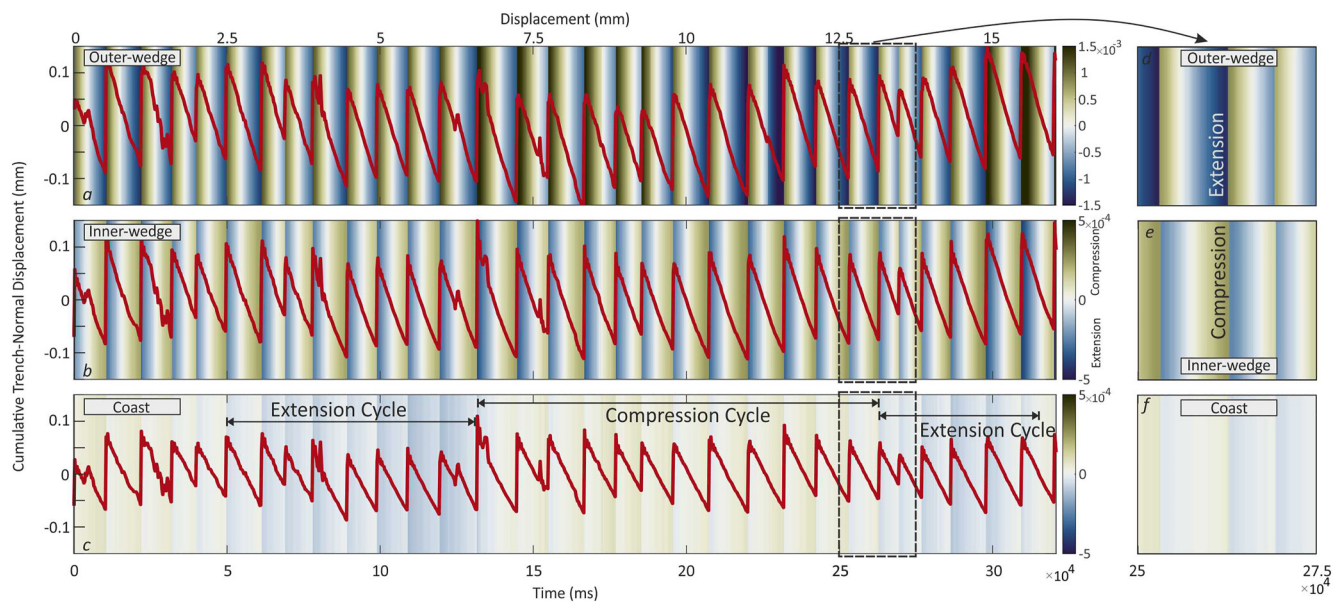


Figure 9. Critical configuration; trench-normal displacement time series (red plot) is overlaid on the strain time series (background color map) over tens of analog earthquake cycles in different segments of the upper plate. The magnitude of the strain in the outer-wedge is one order larger than the inner-wedge and coast. Note that the outer-wedge and inner-wedge show opposite strain states over the earthquake cycle (compressional versus extensional). The compression and extensional supercycles in the coastal region are shown in the lower panel. Please see the text for the discussion.

(Figures 8 and 9). The inner-wedge and coastal wedge are under compression when the outer-wedge is experiencing extension during the interseismic period—this is a general pattern over many seismic cycles. In each cycle, the inner-wedge undergoes extension coseismically, then gradually moves to a neutral state and finally shifts to a stable compressional state and stays in this regime until the next seismic event occurs. In contrast, the outer-wedge is under compression during the earthquake and subsequently experiences neutral and extensional states in the interseismic interval. In both segments, the strain state shows a regular cycle and follows the same earthquake cycle trend.

In the downdip segment, which is treated as underlying the coastal area in our experiment (cf. Figure 1), the strain-state cycle differs from that of the two shallower (offshore) segments of the upper plate. Although the strain magnitude is approximately an order of magnitude smaller, its pattern may be closer to the inner-wedge than to the outer-wedge.

Interestingly, the strain state represents not only an asymmetric cyclic pattern over stick-slip cycles but also a longer cycle (hereafter called “supercycle”; Figures 8 and 9). In the coastal wedge, unlike the other upper plate segments, the extensional and compressional portions of the strain do not balance over a few cycles but show multicycle long compressional and extensional supercycles. The supercycle appears sharper in the critical configuration, where the backthrust is not developed. It may, therefore, be due to the activity (i.e., seismic cycle) of the backthrust that perturbs the supercycle. The surface displacements in the coastal zone and the inner-wedge represent opposite trends (Figure S5 in Supporting Information S1). In the coseismic period, the coast, which overlies the downdip limit of the stick-slip zone, moves trenchward while subsiding (and vice versa in the interseismic period), but the inner-wedge, which overlies the stick-slip zone, moves trenchward while moving upward. This implies that coseismic uplift and subsidence patterns indicate the location of the slipped zone at depth. The possible primary mechanisms for the supercycle will be discussed in Section 4.4.

3.2. Frequency and Size Distributions of Analog Megathrust Events

To explore the possible relationship between moment release patterns and the forearc configurations in our subduction megathrusts, we compare the frequency and size of analog earthquakes and their coefficients of variations (C_v). This coefficient is defined as the ratio of the mean to the standard deviation of the analog megathrust events from both compressional and critical configurations (Kuehn et al., 2008; Rosenau & Oncken, 2009). We have defined a moving window to calculate the coefficient of variation over the size and frequency of events. The coefficient of variation generally exhibits an inverse relationship (i.e., negative correlation) with the periodicity of the frequency-size distribution. In particular, a $C_v > 0.5$ indicates random events while a $C_v < 0.5$ characterizes periodic events.

The results of the size and frequency distribution and temporal evolution of the frequency-size distributions are plotted in Figure 10. Accordingly, the critical configuration is characterized by a relatively larger event size and longer recurrence. In the C_v plots of the compressional configuration (Figures 10c and 10d), a sharp reduction is clear. The slope in the C_v values (Figures 10c and 10d) shows a good agreement with the evolution of the main upper plate structures (i.e., backthrust fault). The C_v of the compressional configuration is generally lower than that of the critical configuration, indicating that the first is more periodic. Although both configurations demonstrate rather periodic behavior (i.e., $C_v < 0.5$), the recurrence pattern of the critical configuration, unlike the compressional configuration, evolves toward higher variability. The C_v values for the critical configuration systematically increase and are characterized by a C_v higher than 0.15. In contrast, in the compressional configuration, the values stay in a range of 0.15–0.2. A similar trend is also observed in the size distributions of both models. The compressional configuration does not show a significant evolution over time; however, an increasing trend is observed toward higher coefficients (i.e., less characteristic events over time) in the critical configuration.

4. Discussion

4.1. Mechanical State of the Shallow Forearc Over the Seismic Cycle

We have used critical wedge theory to design two endmember wedge geometries to see the effect of (transient) instability on the long-term deformation pattern. As shown in Figure 2, the inner-wedges of both models (coastal region in our models) overlying the deeper, creeping megathrust are basically compressional critical

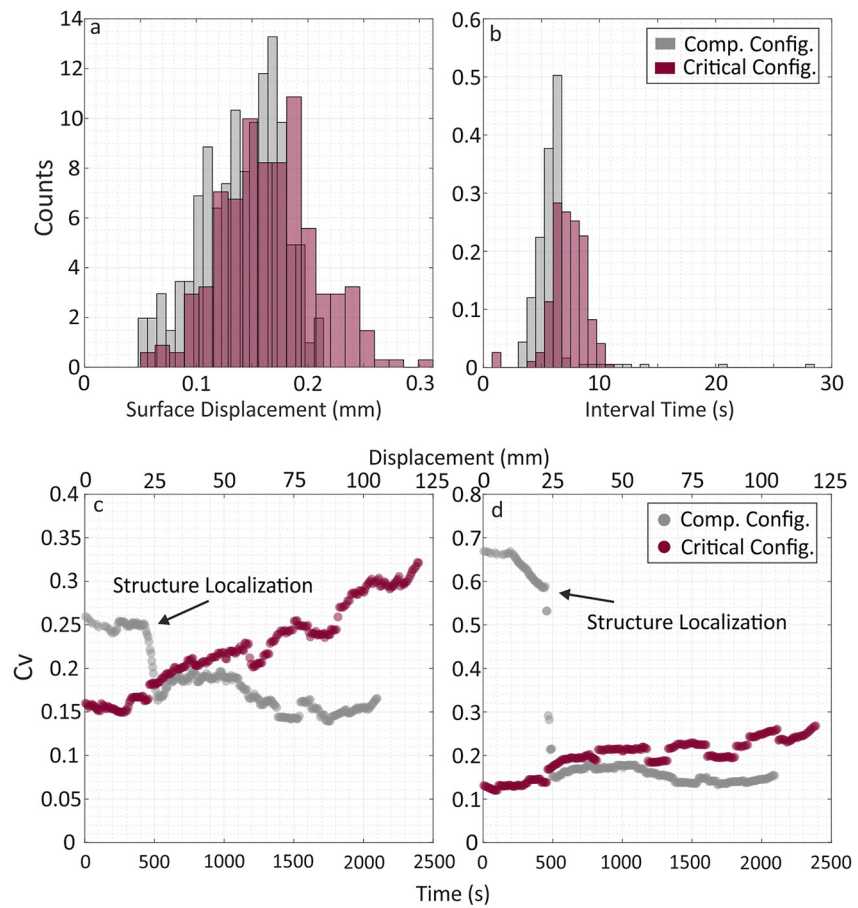


Figure 10. Size and frequency distributions (a) and (b) and coefficients of variation (C_v) of recurrence intervals and size (c) and (d) of analog megathrust events for compressional and critical configurations. Gray and red colors represent compressional and critical configurations. The sharp drops in the C_v values of the compressional configuration are marked by the black arrow.

and expected to deform little as has been observed in the models as well as in nature (e.g., Wang et al., 2019). The part of the wedges overlying the seismogenic zone in both models is, in contrast, predicted to deform at least transiently and in an opposing fashion: The compressional wedge model is compressive only during the interseismic and stable during coseismic periods while the critical configuration is stable interseismically but can reach extensional critical state coseismically depending on how high the stress drop. Such a behavior has been envisioned for the Japan subduction zone in the area of the 2011 Tohoku-Oki earthquake (Wang et al., 2019) and might be most relevant for many active margins where great earthquakes occur. We also note that friction in our analog models, as well as stresses, are generally much higher than in nature, where fluids reduce effective friction along the megathrust dramatically and additional dynamic weakening mechanisms are operating (flash heating, fluid pressurization, etc.).

The outermost-wedge segment of our model, close to the trench and updip of the seismogenic zone, overlies the creeping portion of the interface where slip instability cannot nucleate but may rupture during trench-reaching megathrust events (Cubas et al., 2013a; Noda & Lapusta, 2013). This domain is near the deformation front and undergoes more deformation and splay thrust faulting than the inboard forearc segments. Theoretical and analog earthquake studies suggest that a splay fault at the updip limit of the seismogenic zone may act as a relaxation mechanism for coseismic compression arising from slip tapering toward the trench (Rosenau et al., 2009; Wang & Hu, 2006) and be activated in the early postseismic stage of a seismic cycle. The laboratory observations are in good agreement with the aftershock activities following megathrust events, for instance, after the Maule 2010 (Lieser et al., 2014), Antofagasta 1995 (Pastén-Araya et al., 2021), Iquique 2014 (Soto et al., 2019), and Ecuador-south Colombia 1958 earthquakes (Collot et al., 2004, 2008). This suggests that the large coseismic

displacements on the interface push the outer-wedge to a compressional domain (i.e., shortening; Figure 9; Wang & Hu, 2006; Wang et al., 2019). Consequently, the splay fault between the outer-wedge and inner-wedge may accumulate slip during coseismic or/and postseismic periods.

The inner-wedge is located between this forethrust splay fault and the projection of the downdip limit of the stick-slip zone to the surface or the backthrust upper plate fault (Figure 5). This segment is interseismically stable and accumulate a minimum of permanent deformation (Cubas et al., 2013b). The maximum strain is localized on the backthrust fault, which is the landward boundary of the inner-wedge. However, this backthrust may activate with a normal faulting mechanism during or immediately after a large coseismic slip in the velocity-weakening portion of the interface, similar to the activity of the Pichilemu fault shortly after the Maule 2010 megathrust earthquake (Cubas et al., 2013b; Fariás et al., 2011). This means that the mechanically most stable segment of the entire wedge—i.e., the inner-wedge—reflects the seismically most active (i.e., velocity-weakening) portion of the interface (Fuller et al., 2006).

4.2. Seismotectonic Forearc Segmentation: Comparison With Natural Examples

Our results highlight how coseismic surface deformation may contribute to the morphology of the shallow (offshore: outer-wedge and inner-wedge) segment of the forearc. The coseismic extension that occurs offshore is mainly observed in the inner-wedge, in the zone bounded by the updip forethrust (and/or backthrust) and downdip backthrust (Figure 5). The updip forethrust is the same structure that has been observed in several natural examples. It has been introduced as either backstop in the 2011 Tohoku-Oki earthquake region in the Japan Trench (Ito et al., 2011; Tsuji et al., 2011, 2013) or as the approximate limit between the lower and middle slopes (MLS) in the north Chilean margin (Maksymowicz et al., 2018; Storch et al., 2021). In the former, the fault is characterized by the boundary between a soft and fractured sediment sequence abutting a less-deformed sequence on the landward side. After the 2011 Tohoku-Oki event, seafloor photographs taken from the splay fault (backstop) region show that extensional cliffs are formed coseismically due to small-scale slope failure (Tsuji et al., 2013). We observe similar gravity-induced features in the forelimb of the splay fault in our experiments, indicating the updip limit of the coseismic slip on the interface. Further landward, seafloor photographs from the inner-wedge have suggested coseismic anelastic extensional features with no evidence for submarine landslides and reverse faulting as responsible mechanisms (Tsuji et al., 2013). This segment of the upper plate in both our models and the 2011 Tohoku-Oki event overlies the zone of maximum coseismic slip.

Seafloor extensional features have also been documented in the regions of the Maule 2008 and Iquique 2014 earthquakes in the central and northern Chilean subduction zone (Geersen et al., 2016, 2018; Maksymowicz et al., 2018; Reginato et al., 2020; Storch et al., 2021). A normal faulting escarpment and extensional fractures are observed on the hanging-wall of the forethrust splay in the Maule 2008 earthquake region (Geersen et al., 2016). Although it is not evident whether the normal faults are rooted in the megathrust interface, the extensional fractures (extrado features) on the hanging-wall may be related to the activity of the splay fault. As shown in our model's results, the activity of the splay fault at the updip limit of the rupture area may generate an extensional regime in the hinge zone of the fault-related fold and forms extensional fractures. Note that these frontal splay faults may be active during earthquakes and/or in postseismic intervals. In both cases, however, they indicate the frictional transition zone on the plate interface and, in consequence, the updip limit of the locked seismogenic zone. In line with our model result, the extensional basin between the splay fault (backstop) and the coastal region indicates the megathrust seismogenic zone at depth (Moscoso et al., 2011). The large subduction earthquakes may rupture different portions of the interface from the trench to the downdip end of the seismogenic zone (Lay et al., 2012). Depending on the earthquake magnitude and position of the ruptured segment (i.e., the portion of the megathrust interface beneath the coastal region), the extensional fractures can also be seen onshore as a marker of permanent deformation (Baker et al., 2013; Loveless et al., 2005, 2009).

In the Iquique 2014 earthquake region (north Chilean subduction system), clear evidence of the extensional features in the upper plate has been reported from offshore seismic profiles (Geersen et al., 2018; Reginato et al., 2020; Storch et al., 2021). The offshore extensional features can be categorized into two domains, the Middle-Lower slope transition (MLS) and Middle-Upper slope segments. The former is likely formed by the activity of the large forethrust splay, which may be active during coseismic, postseismic, and interseismic intervals. The Middle-Upper slope segment overlies the main slip zone of the 2014 event. It is possibly formed coseismically and generates the sedimentary basin over hundreds of seismic cycles. This latter correlation also

correlates with the basin-centered gravity lows (e.g., Schurr et al., 2020) that indicate potential asperities at depth (i.e., basin-centered asperities) introduced by Song and Simons (2003) and Wells et al. (2003).

4.3. Forearc Segmentation and Temporal Pattern of Events

The compressional configuration establishes a clear forearc segmentation through forming updip (offshore) splay faults and downdip (onshore) backthrust faults, causing the analog megathrust events to be more regular (same evolution as in Rosenau and Oncken (2009)). Lacking a backthrust, the critical wedge does not have this clear segmentation, while the configuration generates more irregular analog megathrust events. However, the analog earthquake catalogs from both configurations generally represent a periodic behavior, i.e., $C_v < 0.5$. Moreover, the forearc segment bounded by the upper plate faults (forethrust and backthrust) overlies the seismogenic zone; hence, the frontal shortening segment (i.e., inner-wedge) of the compressional configuration behaves as a deterministic spring-slider system (Reid, 1910; Rosenau & Oncken, 2009). In the critical configuration, the extensional fractures on the segment above the seismogenic zone (i.e., inner-wedge) indicate anelastic deformation that correlates with a more complicated temporal pattern of the megathrust events. This is equivalent to the observation of a less periodic pattern of analog earthquakes produced in the critical configuration.

4.4. Coastal Strain Cycle in Response to Earthquake Cycle

In our model, the projection of the downdip limit of the velocity-weakening zone on the surface represents the coastal region (Oleskevich et al., 1999; Ruff & Tichelaar, 1996). Unlike the inner-wedge and outer-wedge, the coastal region reacts in an inhomogeneous pattern to the seismic cycles: its strain state does not only respond to each event (i.e., megathrust earthquake), but the strain state shows a “supercycle” over several cycles. In other words, a “strain switch” from a mostly compressional/extensional to a mostly extensional/compressional state develops over a few cycles (Figures 8 and 9). We hypothesize that internal deformation in the experimentally well-known elastoplastic deformation cycle may be the responsible mechanism for the supercycle. The strain rate in the coastal domain is at least one order of magnitude lower than that in the offshore forearc segments (inner-wedge and outer-wedge); hence, the onshore segment needs more time to reach its yield strength and to shift between mostly compressional/extensional to a mostly extensional/compressional state. This longer strain switch may eventually lead to a more prolonged recurrence of the active upper plate faults inland. These changes in the strain cycles reflect variability in strain rate with respect to the long-term trend such that the compressional wedge is more segmented, and its deformation varies less than the unsegmented critical wedge.

Observations reveal that a relatively low resolution (18 cycles in this case) may provide a good overview of the wedge evolution type as outlined above. However, the details of the cycles and the transient in between can be overprinted, e.g., by the supercycle-related uplift/subsidence and megathrust events involving splay faults. The comparison suggests that the seismic cycle-to-cycle variability causes periodicity in the surface deformation at all (observational) frequencies. The Northwest Coast of the Tohoku-Oki 2011 earthquake (NE Japan; Japan trench) and the Pacific coast of Hokkaido (Kuril trench) have both experienced two different long-term vertical movement histories. In the former case, the Pleistocene marine terrace chronology of the NE coast of Japan has experienced a constant uplift at about 0.2 m/ky (Matsu'ura et al., 2019). In contrast, the Holocene sedimentary succession in the south and central Sanriku (northeast Japan) suggests subsidence at about 1 mm/yr (Niwa et al., 2017). If this opposite long-term coastal vertical movement is accurate enough, it may reflect the coastal strain supercycle in response to the megathrust cycle. In the latter case, the sedimentological investigations and diatom assemblages suggest preseismic submergence at a rate of 8–9 mm/yr (Atwater et al., 2016; Sawai, 2020; Sawai et al., 2004). If this rapid subsidence occurs in each earthquake cycle, megathrust coseismic and postseismic deformation should generate 4–5 m of coastal uplift in each cycle to cancel out the subsidence. A similar subsidence-uplift pattern also occurred in the Aleutian-Alaska subduction system (Shennan & Hamilton, 2006).

This contrast in vertical movement of the coast occurs in subduction systems where the megathrust earthquake usually ruptures the offshore (i.e., shallow) part of the interface (e.g., Japan and Alaska trenches). In the cases where the megathrust earthquakes that partially or fully ruptured the deep part of the interface, for instance, the Antofagasta 1995 (Chlieh et al., 2004; Pritchard et al., 2002) and Illapel 2015 earthquakes (Tilmann et al., 2016) marine terraces recorded a more continuous uplift (with different rates) since the Pleistocene (González-Alfaro et al., 2018). However, a long-term (Miocene) change in the vertical movement has been recorded in some places

Table 1
Summary of Short-Term and Long-Term Forearc Strain State

Configuration	Compressional config.	Compressional config.	Compressional config.	Critical config.	Critical config.	Critical config.
Forearc segment	Coseismic	Interseismic	Long-term permanent	Coseismic	Interseismic	Long-term permanent
Outer-wedge	Compression	From compression moves to a neutral state and finally to extension	Compression	Compression	From compression moves to a neutral state and finally to extension	Compression
Inner-wedge	Extension	From extension moves to a neutral state and finally to a stably compressional	Extensional; extensional zone becomes wider over time	Extension	From extension moves to a neutral state and finally to a stable compressional	Extensional over the seismogenic zone; surface extensional fractures
Coastal region	Extension	Extensional and compressional portions do not balance; asymmetric cyclic pattern	Multicycle long compressional/extensional supercycles	Extension	Extensional and compressional portions do not balance; asymmetric cyclic pattern	Multicycle long compressional/extensional supercycles; sharper supercycle

on the Coastal Cordillera in the Chilean margin, probably caused by basal erosion/accretion sequences (Encinas et al., 2012). This may imply that if the coastal area subsides coseismically but uplifts over the interseismic period, the coast probably overlies the downdip limit of the locked zone while the coastal region may show long-term vertical movement inconsistently. If the coast moves vertically upward during both coseismic and interseismic periods, upper plate thrust faults likely push the coast upward (Clark et al., 2019; Mouslopoulou et al., 2016), and the coastal region continuously accumulates permanent uplift.

Deep slow-slip events, basal accretion, interseismic crustal thickening, and upper plate faulting may enhance coastal uplift at different time scales (Figure S6 in Supporting Information S1; Madella & Ehlers, 2021; Melnick et al., 2018; Menant et al., 2020; Mouslopoulou et al., 2016). Among these processes, underplating may not play a significant portion in a single seismic cycle because the formation of each tectonic slice (i.e., duplex) is in a Myr-scale (Menant et al., 2020; Ruh, 2020). The thermo-mechanical simulations (Menant et al., 2020) suggest early and late stages of a single underplating cycle, respectively, characterized by up to 1.5 mm/yr uplift and subsidence (i.e., re-equilibration of the forearc wedge) rate in the coastal region. This transition from uplift to subsidence (and vice versa) is in the Myr-scale and represents a much lower frequency in comparison with the deformation supercycle observed in our experiments. However, to rule out and differentiate the impact of the different mechanisms involved in the vertical movement of the coastal region, a modeling approach including all the aforementioned mechanisms is needed.

Although the inner-wedge and outer-wedge may show a relatively simple earthquake deformation cycle, the coastal zone in the subduction zones may also show a rather complicated pattern and trend. Where the downdip limit of seismic locking and slip is offshore, both, the deformation resulting from seismic cycle deformation and that from mass flux at the plate interface (subduction erosion versus underplating) generate a composite, more complex kinematic record, even in our simplified seismotectonic model. This implies that predicting the interface behavior from the coastal behavior might not always provide diagnostic evidence in the case of shallow subduction earthquakes where the coast does not overlie the seismogenic zone or its downdip end. Rather, measuring surface deformation above the locked zone provides a more reliable indication of the behavior of the interface.

5. Conclusion

Our results highlight that, in the shallow portion of the subduction zone, frictional properties of the interface and mechanical characteristics of the forearc determine the surface deformation signal over seismic cycles. The mechanical and kinematic interaction between the shallow wedge and the interface can partition the wedge into different segments. These segments may react analogously or oppositely over the different intervals of the seismic cycle (Table 1). Moreover, different wedge segments may switch their strain state from compression/extension

to extension/compression domains. We emphasize that a more segmented upper plate is related to megathrust subduction that generates more characteristic and periodic events.

Our experiments underscore that the stable part of the wedge (i.e., inner-wedge), which undergoes extension coseismically overlies the seismogenic zone. However, the density of extensional fractures and the number of normal faults may increase toward the limit between the inner-wedge and outer-wedge due to the activity of splay faults at the updip limit of the seismogenic zone.

Over a dozen and more analog earthquake cycles, the strain time series reveal that the strain state may switch the mode (extension/compression to compression/extension) after remaining quasi-stable over a few seismic cycles in the coastal zone. Various scenarios have been suggested, such as background seismicity, deep slow-slip events, and subduction accretion/erosion, as the responsible mechanism for switching the kinematic behavior of the coastal domain (uplift to subsidence and vice versa). Here, we additionally show that the mechanical state of the plate interface beneath the coastal region may vary over time and influence the coastal region's strain state. Because the strain rate here is significantly lower than in the offshore segment, this may eventually lead to different observed vertical motions on the coast. Our simplified experiments demonstrate that the strain cycle in the coastal region may show a supercycle pattern superseding the sawtooth pattern of the strain cycles related to the earthquake cycle. This is geodetically relevant as the observations in many subduction zones are focused on the coastal regions. Hence, it may not always be straightforward to use these observations as direct evidence to assess the behavior of the shallow, offshore portion of the megathrust.

Data Availability Statement

All data in this study are online and published open access in Kosari et al. (2022) (<https://doi.org/10.5880/ridgeo.2022.015>). We thank GFZ Data Services for publishing the data.

Acknowledgments

The research was supported by the SUBI-TOP Marie Skłodowska-Curie Action project from the European Union's EU Framework Programme for Research and Innovation Horizon 2020 (Grant Agreement 674899) and Deutsche Forschungsgemeinschaft (DFG) through Grant CRC 1114 "Scaling Cascades in Complex Systems." Project 235221301(B01). The authors thank M. Rudolf, F. Neumann, and Th. Ziegenhagen for their helpful discussion and assistance during our laboratory experiments. We thank the editor of the journal, Laurent Jolivet, and thank Laurent Husson and Nadaya Cubas for their constructive reviews that helped us to greatly improve the paper. The authors also thank Nadaya Cubas for sharing the Matlab code for calculating the CWT stability fields. Some uniform colormaps are adapted from Cramer (2018). Open access funding enabled and organized by Projekt DEAL.

References

- Adam, J., Urai, J. L., Wieneke, B., Oncken, O., Pfeiffer, K., Kukowski, N., et al. (2005). Shear localisation and strain distribution during tectonic faulting—New insights from granular-flow experiments and high-resolution optical image correlation techniques. *Journal of Structural Geology*, 27(2), 283–301. <https://doi.org/10.1016/j.jsg.2004.08.008>
- Atwater, B. F., Furukawa, R., Hemphill-Haley, E., Ikeda, Y., Kashima, K., Kawase, K., et al. (2016). Seventeenth-century uplift in eastern Hokkaido, Japan. *The Holocene*, 14(4), 487–501. <https://doi.org/10.1191/0959683604HL726RP>
- Baker, A., Allmendinger, R. W., Owen, L. A., & Rech, J. A. (2013). Permanent deformation caused by subduction earthquakes in northern Chile. *Nature Geoscience*, 6(6), 492–496. <https://doi.org/10.1038/ngeo1789>
- Caniven, Y., & Dominguez, S. (2021). Validation of a multilayered analog model integrating crust-mantle visco-elastic coupling to investigate subduction megathrust earthquake cycle. *Journal of Geophysical Research: Solid Earth*, 126, e2020JB020342. <https://doi.org/10.1029/2020JB020342>
- Chlieh, M., Avouac, J. P., Sieh, K., Natawidjaja, D. H., & Galetzka, J. (2008). Heterogeneous coupling of the Sumatran megathrust constrained by geodetic and paleogeodetic measurements. *Journal of Geophysical Research*, 113, 5305. <https://doi.org/10.1029/2007JB004981>
- Chlieh, M., De Chabaliere, J. B., Ruegg, J. C., Armijo, R., Dmowska, R., Campos, J., & Feigl, K. L. (2004). Crustal deformation and fault slip during the seismic cycle in the North Chile subduction zone, from GPS and InSAR observations. *Geophysical Journal International*, 158(2), 695–711. <https://doi.org/10.1111/j.1365-246X.2004.02326.x>
- Clark, K., Howarth, J., Litchfield, N., Cochran, U., Turnbull, J., Dowling, L., et al. (2019). Geological evidence for past large earthquakes and tsunamis along the Hikurangi subduction margin, New Zealand. *Marine Geology*, 412, 139–172. <https://doi.org/10.1016/j.margeo.2019.03.004>
- Collot, J.-Y., Agudelo, W., Ribodetti, A., & Marcaillou, B. (2008). Origin of a crustal splay fault and its relation to the seismogenic zone and underplating at the erosional north Ecuador-south Colombia oceanic margin. *Journal of Geophysical Research*, 113, 12102. <https://doi.org/10.1029/2008JB005691>
- Collot, J.-Y., Marcaillou, B., Sage, F., Michaud, F., Agudelo, W., Charvis, P., et al. (2004). Are rupture zone limits of great subduction earthquakes controlled by upper plate structures? Evidence from multichannel seismic reflection data acquired across the northern Ecuador-southwest Colombia margin. *Journal of Geophysical Research*, 109, B11103. <https://doi.org/10.1029/2004JB003060>
- Corbi, F., Bedford, J., Sandri, L., Funicello, F., Gualandi, A., & Rosenau, M. (2020). Predicting imminence of analog megathrust earthquakes with machine learning: Implications for monitoring subduction zones. *Geophysical Research Letters*, 47, e2019GL086615. <https://doi.org/10.1029/2019GL086615>
- Corbi, F., Herrendörfer, R., Funicello, F., & van Dinther, Y. (2017). Controls of seismogenic zone width and subduction velocity on interplate seismicity: Insights from analog and numerical models. *Geophysical Research Letters*, 44, 6082–6091. <https://doi.org/10.1002/2016GL072415>
- Corbi, F., Sandri, L., Bedford, J., Funicello, F., Brizzi, S., Rosenau, M., & Lallemand, S. (2019). Machine learning can predict the timing and size of analog earthquakes. *Geophysical Research Letters*, 46, 1303–1311. <https://doi.org/10.1029/2018GL081251>
- Cramer, F. (2018). *Scientific colour-maps*. <https://doi.org/10.5281/ZENODO.1287763>
- Cubas, N., Avouac, J. P., Leroy, Y. M., & Pons, A. (2013a). Low friction along the high slip patch of the 2011 Mw 9.0 Tohoku-Oki earthquake required from the wedge structure and extensional splay faults. *Geophysical Research Letters*, 40(16), 4231–4237. <https://doi.org/10.1002/grl.50682>
- Cubas, N., Avouac, J. P., Souloumiac, P., & Leroy, Y. (2013b). Megathrust friction determined from mechanical analysis of the forearc in the Maule earthquake area. *Earth and Planetary Science Letters*, 381, 92–103. <https://doi.org/10.1016/j.epsl.2013.07.037>

- Cubas, N., Souloumiac, P., & Singh, S. C. (2016). Relationship link between landward vergence in accretionary prisms and tsunami generation. *Geology*, *44*, 787–790. <https://doi.org/10.1130/G38019.1>
- Dahlen, F. A., Suppe, J., & Davis, D. (1984). Mechanics of fold-and-thrust belts and accretionary wedges: Cohesive Coulomb Theory. *Journal of Geophysical Research*, *89*(B12), 10087–10101. <https://doi.org/10.1029/JB089IB12P10087>
- Davis, D., Suppe, J., & Dahlen, F. A. (1983). Mechanics of fold-and-thrust belts and accretionary wedges. *Journal of Geophysical Research*, *88*(B2), 1153–1172. <https://doi.org/10.1029/JB088IB02P01153>
- Delano, J. E., Amos, C. B., Loveless, J. P., Rittenour, T. M., Sherrod, B. L., & Lynch, E. M. (2017). Influence of the megathrust earthquake cycle on upper-plate deformation in the Cascadia forearc of Washington State, USA. *Geology*, *45*(11), 1051–1054. <https://doi.org/10.1130/G39070.1>
- Encinas, A., Finger, K. L., Buatois, L. A., & Peterson, D. E. (2012). Major forearc subsidence and deep-marine miocene sedimentation in the present coastal Cordillera and longitudinal depression of south-central Chile (38°30'S–41°45'S). *GSA Bulletin*, *124*(7–8), 1262–1277. <https://doi.org/10.1130/B30567.1>
- Fariás, M., Comte, D., Roecker, S., Carrizo, D., & Pardo, M. (2011). Crustal extensional faulting triggered by the 2010 Chilean earthquake: The Pichilemu seismic sequence. *Tectonics*, *30*, TC6010. <https://doi.org/10.1029/2011TC002888>
- Fuller, C. W., Willett, S. D., & Brandon, M. T. (2006). Formation of forearc basins and their influence on subduction zone earthquakes. *Geology*, *34*(2), 65–68. <https://doi.org/10.1130/G21828.1>
- Geersen, J., Ranero, C. R., Klaucke, I., Behrmann, J. H., Kopp, H., Tréhu, A. M., et al. (2018). Active tectonics of the north Chilean marine forearc and adjacent oceanic Nazca Plate. *Tectonics*, *37*, 4194–4211. <https://doi.org/10.1029/2018TC005087>
- Geersen, J., Scholz, F., Linke, P., Schmidt, M., Lange, D., Behrmann, J. H., et al. (2016). Fault zone controlled seafloor methane seepage in the rupture area of the 2010 Maule earthquake, Central Chile. *Geochemistry, Geophysics, Geosystems*, *17*, 4802–4813. <https://doi.org/10.1002/2016GC006498>
- González-Alfaro, J., Vargas, G., Ortlieb, L., González, G., Ruiz, S., Báez, J. C., et al. (2018). Abrupt increase in the coastal uplift and earthquake rate since ~40 ka at the northern Chile seismic gap in the Central Andes. *Earth and Planetary Science Letters*, *502*, 32–45. <https://doi.org/10.1016/j.epsl.2018.08.043>
- Ito, Y., Tsuji, T., Osada, Y., Kido, M., Inazu, D., Hayashi, Y., et al. (2011). Frontal deformation near the source region of the 2011 Tohoku-Oki earthquake. *Geophysical Research Letters*, *38*, L00G05. <https://doi.org/10.1029/2011GL048355>
- Jara-Muñoz, J., Melnick, D., Brill, D., & Strecker, M. R. (2015). Segmentation of the 2010 Maule Chile earthquake rupture from a joint analysis of uplifted marine terraces and seismic-cycle deformation patterns. *Quaternary Science Reviews*, *113*(1), 171–192. <https://doi.org/10.1016/j.quascirev.2015.01.005>
- King Hubbert, M. (1937). Theory of scale models as applied to the study of geologic structures. *Bulletin of the Geological Society of America*, *48*(10), 1459–1520. <https://doi.org/10.1130/GSAB-48-1459>
- Kopp, H. (2013). Invited review paper: The control of subduction zone structural complexity and geometry on margin segmentation and seismicity. *Tectonophysics*, *589*, 1–16. <https://doi.org/10.1016/j.tecto.2012.12.037>
- Kosari, E., Rosenau, M., Bedford, J., Rudolf, M., & Oncken, O. (2020). On the relationship between offshore geodetic coverage and slip model uncertainty: Analog megathrust earthquake case studies. *Geophysical Research Letters*, *47*, e2020GL088266. <https://doi.org/10.1029/2020GL088266>
- Kosari, E., Rosenau, M., & Oncken, O. (2022). Digital image correlation data from laboratory subduction megathrust models. *GFZ Data Services*. <https://doi.org/10.5880/figeo.2022.015>
- Kuehn, N. M., Hainzl, S., & Scherbaum, F. (2008). Non-Poissonian earthquake occurrence in coupled stress release models and its effect on seismic hazard. *Geophysical Journal International*, *174*(2), 649–658. <https://doi.org/10.1111/j.1365-246X.2008.03835.X>
- Lay, T., Kanamori, H., Ammon, C. J., Koper, K. D., Hutko, A. R., Ye, L., et al. (2012). Depth-varying rupture properties of subduction zone megathrust faults. *Journal of Geophysical Research*, *117*, B04311. <https://doi.org/10.1029/2011JB009133>
- Lieser, K., Grevemeyer, I., Lange, D., Flueh, E., Tilmann, F., & Contreras-Reyes, E. (2014). Splay fault activity revealed by aftershocks of the 2010 Mw 8.8 Maule earthquake, central Chile. *Geology*, *42*(9), 823–826. <https://doi.org/10.1130/G35848.1>
- Loveless, J. P., Allmendinger, R. W., Pritchard, M. E., Garroway, J. L., & González, G. (2009). Surface cracks record long-term seismic segmentation of the Andean margin. *Geology*, *37*(1), 23–26. <https://doi.org/10.1130/G25170A.1>
- Loveless, J. P., Hoke, G. D., Allmendinger, R. W., González, G., Isacks, B. L., & Carrizo, D. A. (2005). Pervasive cracking of the northern Chilean Coastal Cordillera: New evidence for forearc extension. *Geology*, *33*(12), 973–976. <https://doi.org/10.1130/G22004.1>
- Loveless, J. P., & Meade, B. J. (2011). Spatial correlation of interseismic coupling and coseismic rupture extent of the 2011 MW = 9.0 Tohoku-Oki earthquake. *Geophysical Research Letters*, *38*, L17306. <https://doi.org/10.1029/2011GL048561>
- Madella, A., & Ehlers, T. A. (2021). Contribution of background seismicity to forearc uplift. *Nature Geoscience*, *14*, 620–625. <https://doi.org/10.1038/s41561-021-00779-0>
- Maksymowicz, A., Ruiz, J., Vera, E., Contreras-Reyes, E., Ruiz, S., Arraigada, C., et al. (2018). Heterogeneous structure of the Northern Chile marine forearc and its implications for megathrust earthquakes. *Geophysical Journal International*, *215*(2), 1080–1097. <https://doi.org/10.1093/gji/ggy325>
- Malatesta, L. C., Bruhat, L., Finnegan, N. J., & Olive, J.-A. L. (2021). Co-location of the downdip end of seismic coupling and the continental shelf break. *Journal of Geophysical Research: Solid Earth*, *126*, e2020JB019589. <https://doi.org/10.1029/2020JB019589>
- Matsu'ura, T., Komatsubara, J., & Wu, C. (2019). Accurate determination of the Pleistocene uplift rate of the NE Japan forearc from the buried MIS 5e marine terrace shoreline angle. *Quaternary Science Reviews*, *212*, 45–68. <https://doi.org/10.1016/j.quascirev.2019.03.007>
- Melnick, D., Bookhagen, B., Strecker, M. R., & Echtler, H. P. (2009). Segmentation of megathrust rupture zones from fore-arc deformation patterns over hundreds to millions of years, Arauco peninsula, Chile. *Journal of Geophysical Research*, *114*, B01407. <https://doi.org/10.1029/2008JB005788>
- Melnick, D., Li, S., Moreno, M., Cisternas, M., Jara-Muñoz, J., Wesson, R., et al. (2018). Back to full interseismic plate locking decades after the giant 1960 Chile earthquake. *Nature Communications*, *9*(1), 3527. <https://doi.org/10.1038/s41467-018-05989-6>
- Menant, A., Angiboust, S., Gerya, T., Lacassin, R., Simoes, M., & Grandin, R. (2020). Transient stripping of subducting slabs controls periodic forearc uplift. *Nature Communications*, *11*(1), 1823. <https://doi.org/10.1038/s41467-020-15580-7>
- Métouis, M., Socquet, A., Vigny, C., Carrizo, D., Peyrat, S., Delorme, A., et al. (2013). Revisiting the North Chile seismic gap segmentation using GPS-derived interseismic coupling. *Geophysical Journal International*, *194*(3), 1283–1294. <https://doi.org/10.1093/gji/fgt183>
- Molina, D., Tassara, A., Abarca, R., Melnick, D., & Madella, A. (2021). Frictional segmentation of the Chilean megathrust from a multivariate analysis of geophysical, geological, and geodetic data. *Journal of Geophysical Research: Solid Earth*, *126*, e2020JB020647. <https://doi.org/10.1029/2020JB020647>
- Moreno, M., Rosenau, M., & Oncken, O. (2010). 2010 Maule earthquake slip correlates with pre-seismic locking of Andean subduction zone. *Nature*, *467*(7312), 198–202. <https://doi.org/10.1038/nature09349>

- Moscoco, E., Grevemeyer, I., Contreras-Reyes, E., Flueh, E. R., Dzierma, Y., Rabbal, W., & Thorwart, M. (2011). Revealing the deep structure and rupture plane of the 2010 Maule, Chile earthquake ($M_w = 8.8$) using wide angle seismic data. *Earth and Planetary Science Letters*, 307(1–2), 147–155. <https://doi.org/10.1016/j.epsl.2011.04.025>
- Mouslopoulou, V., Oncken, O., Hainzl, S., & Nicol, A. (2016). Uplift rate transients at subduction margins due to earthquake clustering. *Tectonics*, 35, 2370–2384. <https://doi.org/10.1002/2016TC004248>
- Niwa, Y., Sugai, T., Matsushima, Y., & Toda, S. (2017). Subsidence along the central to southern Sanriku coast, northeast Japan, near the source region of the 2011 Tohoku-Oki earthquake, estimated from the Holocene sedimentary succession along a ria coast. *Quaternary International*, 456, 1–16. <https://doi.org/10.1016/j.quaint.2017.08.008>
- Noda, H., & Lapusta, N. (2013). Stable creeping fault segments can become destructive as a result of dynamic weakening. *Nature*, 493(7433), 518–521. <https://doi.org/10.1038/nature11703>
- Normand, R., Simpson, G., Herman, F., Haque Biswas, R., Bahroudi, A., & Schneider, B. (2019). Dating and morpho-stratigraphy of uplifted marine terraces in the Makran subduction zone (Iran). *Earth Surface Dynamics*, 7(1), 321–344. <https://doi.org/10.5194/ESURF-7-321-2019>
- Oleskevich, D. A., Hyndman, R. D., & Wang, K. (1999). The updip and downdip limits to great subduction earthquakes: Thermal and structural models of Cascadia, south Alaska, SW Japan, and Chile. *Journal of Geophysical Research*, 104(B7), 14965–14991. <https://doi.org/10.1029/1999JB900060>
- Ott, R. F., Gallen, S. F., Wegmann, K. W., Biswas, R. H., Herman, F., & Willett, S. D. (2019). Pleistocene terrace formation, Quaternary rock uplift rates and geodynamics of the Hellenic Subduction Zone revealed from dating of paleoshorelines on Crete, Greece. *Earth and Planetary Science Letters*, 525, 115757. <https://doi.org/10.1016/j.epsl.2019.115757>
- Ozawa, S., Nishimura, T., Suito, H., Kobayashi, T., Tobita, M., & Imakiire, T. (2011). Coseismic and postseismic slip of the 2011 magnitude-9 Tohoku-Oki earthquake. *Nature*, 475(7356), 373–376. <https://doi.org/10.1038/nature10227>
- Pastén-Araya, F., Potin, B., Ruiz, S., Zerbást, L., Aden-Antoniów, F., Azúa, K., et al. (2021). Seismicity in the upper plate of the Northern Chilean offshore forearc: Evidence of splay fault south of the Mejillones Peninsula. *Tectonophysics*, 800, 228706. <https://doi.org/10.1016/j.tecto.2020.228706>
- Pritchard, M. E., Simons, M., Rosen, P. A., Hensley, S., & Webb, F. H. (2002). Co-seismic slip from the 1995 July 30 $M_w = 8.1$ Antofagasta, Chile, earthquake as constrained by InSAR and GPS observations. *Geophysical Journal International*, 150(2), 362–376. <https://doi.org/10.1046/j.1365-246X.2002.01661.x>
- Reginato, G., Vera, E., Contreras-Reyes, E., Tréhu, A. M., Maksymowicz, A., Bello-González, J. P., & González, F. (2020). Seismic structure and tectonics of the continental wedge overlying the source region of the Iquique $M_w 8.1$ 2014 earthquake. *Tectonophysics*, 796, 228629. <https://doi.org/10.1016/j.tecto.2020.228629>
- Reid, H. F. (1910). *The mechanism of the Earthquake, the California Earthquake of April 18, 1906, Report of the State Earthquake Investigation Commission* (Vol. 2). Washington, DC: Carnegie Institution.
- Rosenau, M., Corbi, F., & Dominguez, S. (2017). Analogue earthquakes and seismic cycles: Experimental modelling across timescales. *Solid Earth, European Geosciences Union*, 8(3), 597–635. <https://doi.org/10.5194/se-8-597-2017>
- Rosenau, M., Horenko, I., Corbi, F., Rudolf, M., Kornhuber, R., & Oncken, O. (2019). Synchronization of great subduction megathrust earthquakes: Insights from scale model analysis. *Journal of Geophysical Research: Solid Earth*, 124, 3646–3661. <https://doi.org/10.1029/2018JB016597>
- Rosenau, M., Lohrmann, J., & Oncken, O. (2009). Shocks in a box: An analogue model of subduction earthquake cycles with application to seismotectonic forearc evolution. *Journal of Geophysical Research*, 114, B01409. <https://doi.org/10.1029/2008JB005665>
- Rosenau, M., Nerlich, R., Brune, S., & Oncken, O. (2010). Experimental insights into the scaling and variability of local tsunamis triggered by giant subduction megathrust earthquakes. *Journal of Geophysical Research*, 115, B09314. <https://doi.org/10.1029/2009JB007100>
- Rosenau, M., & Oncken, O. (2009). Fore-arc deformation controls frequency-size distribution of megathrust earthquakes in subduction zones. *Journal of Geophysical Research*, 114, B10311. <https://doi.org/10.1029/2009JB006359>
- Ruff, L. J., & Tichelaar, B. W. (1996). What controls the seismogenic plate interface in subduction zones? *Geophysical Monograph Series*, 96, 105–111. <https://doi.org/10.1029/GM096P0105>
- Ruh, J. B. (2020). Numerical modeling of tectonic underplating in accretionary wedge systems. *Geosphere*, 16(6), 1385–1407. <https://doi.org/10.1130/GES02273.1>
- Saillard, M., Audin, L., Rousset, B., Avouac, J.-P., Chlieh, M., Hall, S. R., et al. (2017). From the seismic cycle to long-term deformation: Linking seismic coupling and quaternary coastal geomorphology along the Andean megathrust. *Tectonics*, 36, 241–256. <https://doi.org/10.1002/2016TC004156>
- Sawai, Y. (2020). Subduction zone paleoseismology along the Pacific coast of northeast Japan—Progress and remaining problems. *Earth-Science Reviews*, 208, 103261. <https://doi.org/10.1016/j.earscirev.2020.103261>
- Sawai, Y., Satake, K., Kamataki, T., Nasu, H., Shishikura, M., Atwater, B. F., et al. (2004). Transient uplift after a 17th-century earthquake along the Kuril subduction zone. *Science*, 306(5703), 1918–1920. <https://doi.org/10.1126/SCIENCE.1104895>
- Schmalzle, G. M., McCaffrey, R., & Creager, K. C. (2014). Central Cascadia subduction zone creep. *Geochemistry, Geophysics, Geosystems*, 15, 1515–1532. <https://doi.org/10.1002/2013GC005172>
- Schurr, B., Moreno, M., Tréhu, A. M., Bedford, J., Kummerow, J., Li, S., & Oncken, O. (2020). Forming a mogi doughnut in the years prior to and immediately before the 2014 $M_w 8.1$ Iquique, northern Chile, earthquake. *Geophysical Research Letters*, 47, e2020GL088351. <https://doi.org/10.1029/2020GL088351>
- Shennan, I., & Hamilton, S. (2006). Coseismic and pre-seismic subsidence associated with great earthquakes in Alaska. *Quaternary Science Reviews*, 25(1–2), 1–8. <https://doi.org/10.1016/j.quascirev.2005.09.002>
- Simons, M., Minson, S. E., Sladen, A., Ortega, F., Jiang, J., Owen, S. E., et al. (2011). The 2011 magnitude 9.0 Tohoku-Oki earthquake: Mosaicking the megathrust from seconds to centuries. *Science*, 332(6036), 1421–1425. <https://doi.org/10.1126/SCIENCE.1206731>
- Song, T. R. A., & Simons, M. (2003). Large trench-parallel gravity variations predict seismogenic behavior in subduction zones. *Science*, 301(5633), 630–633. <https://doi.org/10.1126/science.1085557>
- Soto, H., Sippl, C., Schurr, B., Kummerow, J., Asch, G., Tilmann, F., et al. (2019). Probing the northern Chile megathrust with seismicity: The 2014 $M_w 8.1$ Iquique earthquake sequence. *Journal of Geophysical Research: Solid Earth*, 124, 12935–12954. <https://doi.org/10.1029/2019JB017794>
- Storch, I., Buske, S., Victor, P., & Oncken, O. (2021). Seismic images of the Northern Chilean subduction zone at 19°40'S, prior to the 2014 Iquique earthquake. *Geophysical Journal International*, 225(2), 1048–1061. <https://doi.org/10.1093/gji/ggab035>
- Sun, T., Wang, K., Fujiwara, T., Kodaira, S., & He, J. (2017). Large fault slip peaking at trench in the 2011 Tohoku-Oki earthquake. *Nature Communications*, 8(1), 14044. <https://doi.org/10.1038/ncomms14044>
- Tilmann, F., Zhang, Y., Moreno, M., Saul, J., Eckelmann, F., Palo, M., et al. (2016). The 2015 Illapel earthquake, central Chile: A type case for a characteristic earthquake? *Geophysical Research Letters*, 43, 574–583. <https://doi.org/10.1002/2015GL066963>

- Tsuji, T., Ito, Y., Kido, M., Osada, Y., Fujimoto, H., Ashi, J., et al. (2011). Potential tsunamigenic faults of the 2011 off the Pacific coast of Tohoku Earthquake. *Earth, Planets and Space*, *63*(7), 831–834. <https://doi.org/10.5047/EPS.2011.05.028>
- Tsuji, T., Kawamura, K., Kanamatsu, T., Kasaya, T., Fujikura, K., Ito, Y., et al. (2013). Extension of continental crust by anelastic deformation during the 2011 Tohoku-Oki earthquake: The role of extensional faulting in the generation of a great tsunami. *Earth and Planetary Science Letters*, *364*, 44–58. <https://doi.org/10.1016/j.epsl.2012.12.038>
- Wallace, L. M., Barnes, P., Beavan, J., Dissen, R., VanLitchfield, N., Litchfield, J., et al. (2012). The kinematics of a transition from subduction to strike-slip: An example from the central New Zealand plate boundary. *Journal of Geophysical Research*, *117*, B02405. <https://doi.org/10.1029/2011JB008640>
- Wang, K., Brown, L., Hu, Y., Yoshida, K., He, J., & Sun, T. (2019). Stable forearc stressed by a weak megathrust: Mechanical and geodynamic implications of stress changes caused by the M = 9 Tohoku-Oki earthquake. *Journal of Geophysical Research: Solid Earth*, *124*, 6179–6194. <https://doi.org/10.1029/2018JB017043>
- Wang, K., & Hu, Y. (2006). Accretionary prisms in subduction earthquake cycles: The theory of dynamic Coulomb wedge. *Journal of Geophysical Research*, *111*, B06410. <https://doi.org/10.1029/2005JB004094>
- Wells, R. E., Blakely, R. J., Sugiyama, Y., Scholl, D. W., & Dinterman, P. A. (2003). Basin-centered asperities in great subduction zone earthquakes: A link between slip, subsidence, and subduction erosion? *Journal of Geophysical Research*, *108*(B10), 2507. <https://doi.org/10.1029/2002JB002072>
- Williamson, A. L., & Newman, A. V. (2018). Limitations of the resolvability of finite-fault models using static land-based geodesy and open-ocean tsunami waveforms. *Journal of Geophysical Research: Solid Earth*, *123*, 9033–9048. <https://doi.org/10.1029/2018JB016091>

References From the Supporting Information

- Herman, M. W., & Govers, R. (2020). Stress evolution during the megathrust earthquake cycle and its role in triggering extensional deformation in subduction zones. *Earth and Planetary Science Letters*, *544*, 116379. <https://doi.org/10.1016/j.epsl.2020.116379>
- Moreno, M. S., Bolte, J., Klotz, J., & Melnick, D. (2009). Impact of megathrust geometry on inversion of coseismic slip from geodetic data: Application to the 1960 Chile earthquake. *Geophysical Research Letters*, *36*, L16310. <https://doi.org/10.1029/2009GL039276>
- Wang, K., & Tréhu, A. M. (2016). Invited review paper: Some outstanding issues in the study of great megathrust earthquakes—The Cascadia example. *Journal of Geodynamics*, *98*, 1–18. <https://doi.org/10.1016/j.jog.2016.03.010>